

1
2
3
4
5
6
7
8
9
10
11
12
13
14
15
16
17
18
19
20
21

Supporting Information (SI) on

Carboxymethyl cellulose modified magnetic bentonite composite for efficient enrichment of radionuclides

Rui Hu^{a,b}, Xuemei Ren^{b,*}, Guangshun Hou^c, Dadong Shao^{b,*}, Yu Gong^d, Xiaojun Chen^d,
Xiaoli Tan^b, Xiangke Wang^e, Masaaki Nagatsu^a

^aGraduate School of Science and Technology, Shizuoka University, Hamamatsu, 432-
8561, Japan

^bInstitute of Plasma Physics, Chinese Academy of Sciences, P.X. Box 1126, Hefei
230031, P.R. China

^cInstitute of Resources & Environment, Henan Polytechnic University, Jiaozuo 454003,
P.R. China

^dInstitute of Nuclear physics and Chemistry, China Academy of Engineering Physics,
Mianyang 621900, PR China

^eSchool of Environment and Chemical Engineering, North China Electric Power
University, Beijing 102206, P.R. China

*Corresponding author: Tel: +86-551-65593308. Fax: +86-551-65591310.

E-mail: xmren@ipp.ac.cn (X.M. Ren), shaodadong@126.com (D.D Shao).

24 **1. Models of adsorption kinetics**

25 The kinetic results were modeled by the pseudo-first-order and pseudo-second-order
26 rate equations, showing as follows:¹

27
$$\log(Q_e - Q_t) = \log Q_e - \frac{k_1}{2.303} t \quad (1)$$

28
$$\frac{t}{Q_t} = \frac{1}{2K'Q_e^2} + \frac{t}{Q_e} \quad (2)$$

29 where Q_e ($\text{mg}\cdot\text{g}^{-1}$) and Q_t ($\text{mg}\cdot\text{g}^{-1}$) are the amount of radionuclides enriched at
30 equilibrium and specific time t (h). k_1 (h^{-1}) and K' ($\text{g}\cdot\text{mg}^{-1}\cdot\text{h}^{-1}$) are the kinetic rate
31 constants of two equations, respectively.

32 **2. Langmuir and Freundlich isotherm models**

33 Langmuir adsorption isotherm model assumes that the adsorbent surfaces provide
34 homogeneous binding sites and equivalent adsorption energies, and there is no interaction
35 between adsorbed species.² It is always applied to describe monolayer adsorption
36 behavior in different systems, and can be expressed in the following form:

37
$$\frac{C_e}{Q_s} = \frac{1}{K_L Q_{s,\max}} + \frac{C_e}{Q_{s,\max}} \quad (3)$$

38 where Q_s ($\text{mg}\cdot\text{g}^{-1}$) is the amount of enriched radionuclides on CMC-g-MB composite,
39 $Q_{s,\max}$ ($\text{mg}\cdot\text{g}^{-1}$) is the maximum of enriched radionuclides per unit weight of CMC-g-MB
40 composite on the complete monolayer coverage, K_L ($\text{L}\cdot\text{mg}^{-1}$) is the Langmuir adsorption
41 coefficient implying adsorption enthalpy and varies with temperatures.

42 As an empirical equation, Freundlich isotherm model is based on the adsorption
43 behavior occurred on heterogeneous surfaces, and is expressed by Eq. (4):

44
$$\log Q_s = \log K_F + \frac{1}{n} \log C_e \quad (4)$$

45 where K_F ($\text{mg}^{1-n}\cdot\text{L}^n\cdot\text{g}^{-1}$) is the Freundlich adsorption coefficient correlated with
46 adsorption capacity and $1/n$ is an index of isotherm non-linearity correlated with to the
47 adsorption intensity at specific temperatures.³

48 **3. Adsorption thermodynamics**

49 The adsorption amounts of Cs(I), Sr(II) and Co(II) on CMC-g-MB composite increase
50 as the temperature increases from 298 K to 338 K. Thermodynamic parameters including

51 average standard enthalpy change (ΔH^0), standard entropy change (ΔS^0) and standard
52 Gibbs free energy change (ΔG^0) of radionuclide adsorption on CMC-g-MB composite are
53 calculated from the temperature-dependent adsorption isotherms. ΔG^0 is expressed as the
54 following function:

$$55 \quad \Delta G^0 = -RT \ln K^0 \quad (5)$$

56 where R is the ideal gas constant ($8.314 \text{ J}\cdot\text{mol}^{-1}\cdot\text{K}^{-1}$), K^0 is the adsorption equilibrium
57 constant standing for the adsorption abilities of CMC-g-MB composite towards
58 radionuclides. The values of $\ln K^0$ can be obtained by plotting $\ln K_d$ versus C_e for
59 radionuclide adsorption and then extrapolating C_e to zero (Fig. S5).

60 ΔH^0 and ΔS^0 can be achieved the slope and intercept of the plots of $\ln K^0$ versus $1/T$ by

61 Eq. (6):

$$62 \quad \Delta S^0 = - \left(\frac{\partial G^0}{\partial T} \right)_P \quad (6)$$

$$63 \quad \ln K^0 = \frac{\Delta S^0}{R} - \frac{\Delta H^0}{RT} \quad (7)$$

64 Linear plots of $\ln K^0$ versus $1/T$ for Cs(I), Sr(II) and Co(II) adsorption on CMC-g-MB
65 composite are shown in Fig. S5D.

66 **Table S1.** Parameters for kinetic models.

Model	Parameters	Cs(I)	Sr(II)	Co(II)
Pseudo first order	k_f (h^{-1})	0.217	0.220	0.215
	Q_e ($\text{mg}\cdot\text{g}^{-1}$)	74.6	59.2	38.9
	R^2	0.948	0.946	0.953
Pseudo second order	K' ($\text{g}\cdot\text{mg}^{-1}\cdot\text{h}^{-1}$)	0.016	0.012	0.031
	Q_e ($\text{mg}\cdot\text{g}^{-1}$)	79.7	62.5	40.2
	R^2	0.999	0.999	0.999
	$Q_{e,exp}^a$ ($\text{mg}\cdot\text{g}^{-1}$)	80.5	63.0	41.1

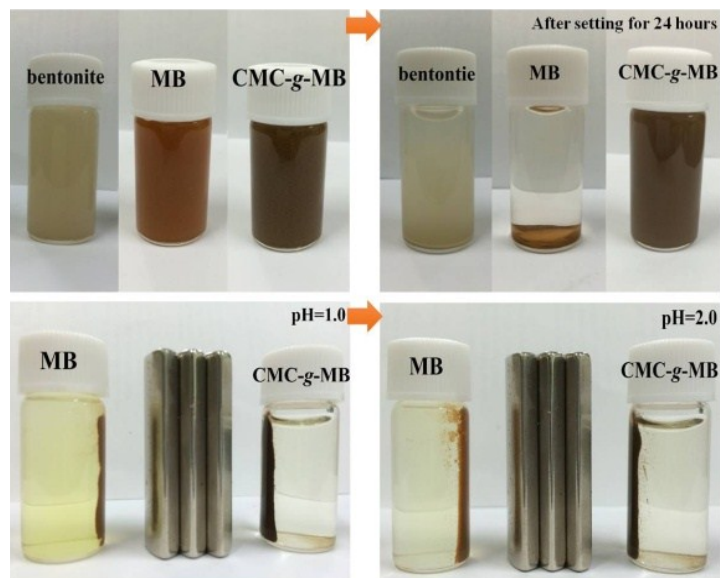
67 ^a $Q_{e,exp}$ is the experimental value of adsorption capacity.

68

69 **Table S2.** Parameters simulated from Langmuir and Freundlich models.

Experimental conditions	Langmuir model			Freundlich model			
	$Q_{s,max}$ ($\text{mg}\cdot\text{L}^{-1}$)	K_L ($\text{L}\cdot\text{mg}^{-1}$)	R^2	K_F ($\text{mg}^{1-n}\cdot\text{L}^n\cdot\text{g}^{-1}$)	1/n	R^2	
CMC-g-MB							
Cs(I)	298 K	80.5	0.468	0.996	29.9	0.319	0.899
	318 K	87.7	0.497	0.995	33.0	0.321	0.929
	338 K	96.7	0.508	0.998	36.4	0.333	0.966
Sr(II)	298 K	63.0	0.299	0.995	19.9	0.336	0.936
	318 K	71.2	0.285	0.996	21.3	0.359	0.945
	338 K	81.4	0.302	0.999	24.5	0.370	0.948
Co(II)	298 K	41.1	0.373	0.991	16.1	0.271	0.910
	318 K	49.7	0.327	0.994	17.3	0.302	0.948
	338 K	64.8	0.272	0.996	19.9	0.343	0.963
MB							
Cs(I)	298 K	48.5	0.250	0.991	13.7	0.368	0.904
Sr(II)	298 K	39.5	0.070	0.996	5.60	0.483	0.957
Co(II)	298 K	26.3	0.065	0.986	3.37	0.505	0.930

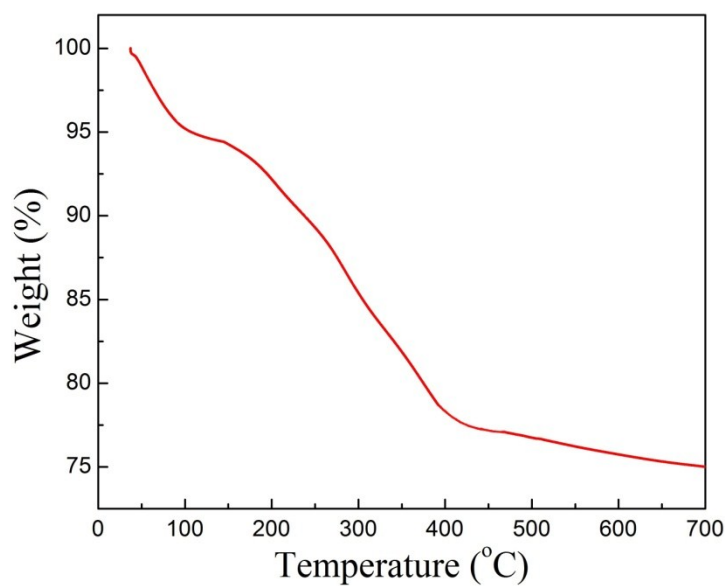
70



71

72 **Fig. S1.** Dispersion images of bentonite, MB and CMC-g-MB composite (settling for 24
73 hours), and stability evaluation of MB and CMC-g-MB composite in acid conditions.

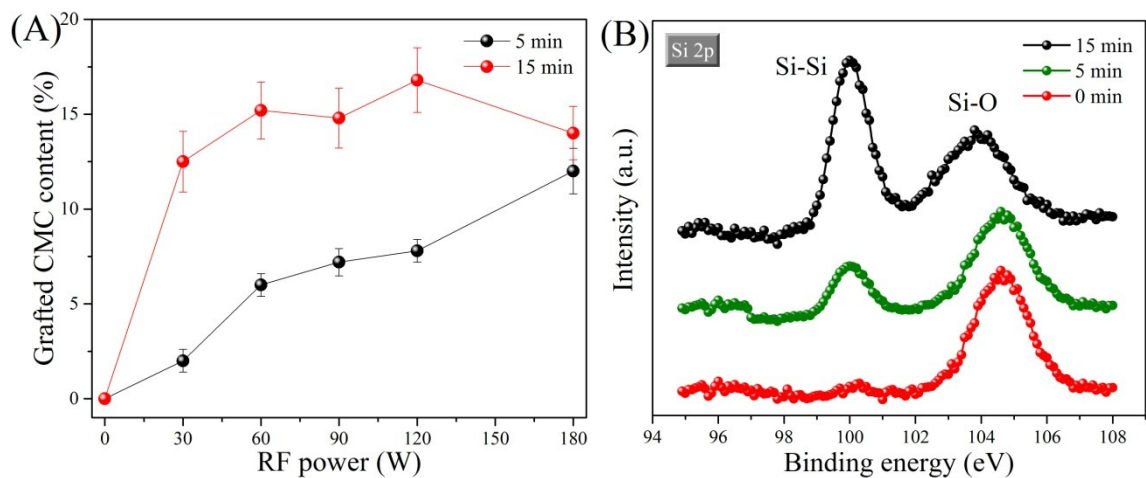
74



75

76

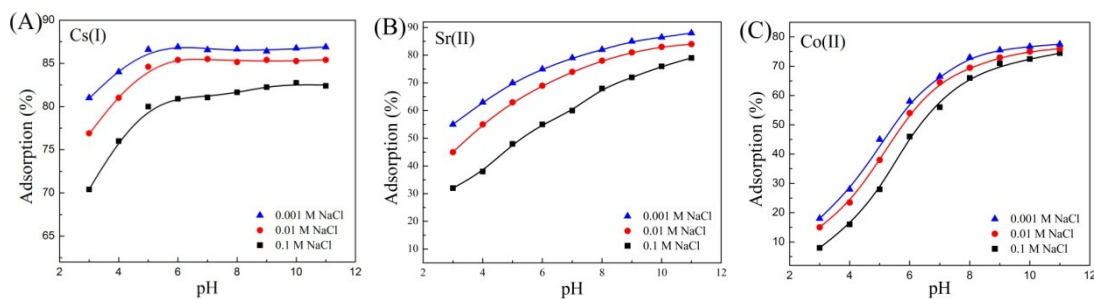
Fig. S2. Typical TGA curve of CMC-g-MB composite.



77

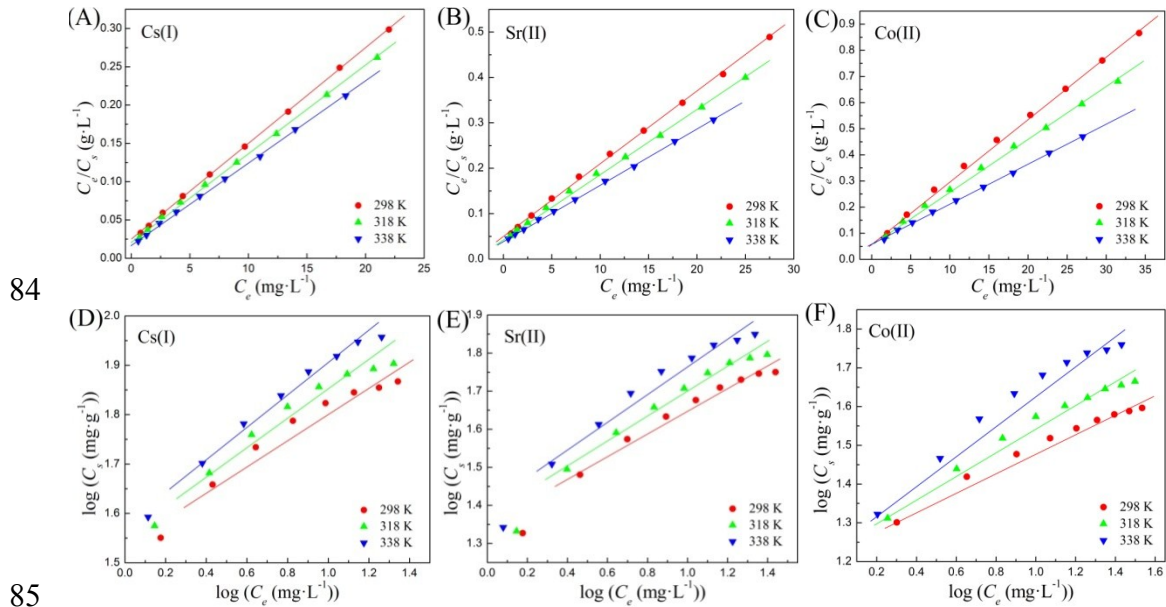
78 **Fig. S3.** Influences of RF power and time on the CMC grafting content (A); XPS Si 2p
 79 spectra of CMC-g-MB composite treated with different duration times of RF plasma (B).

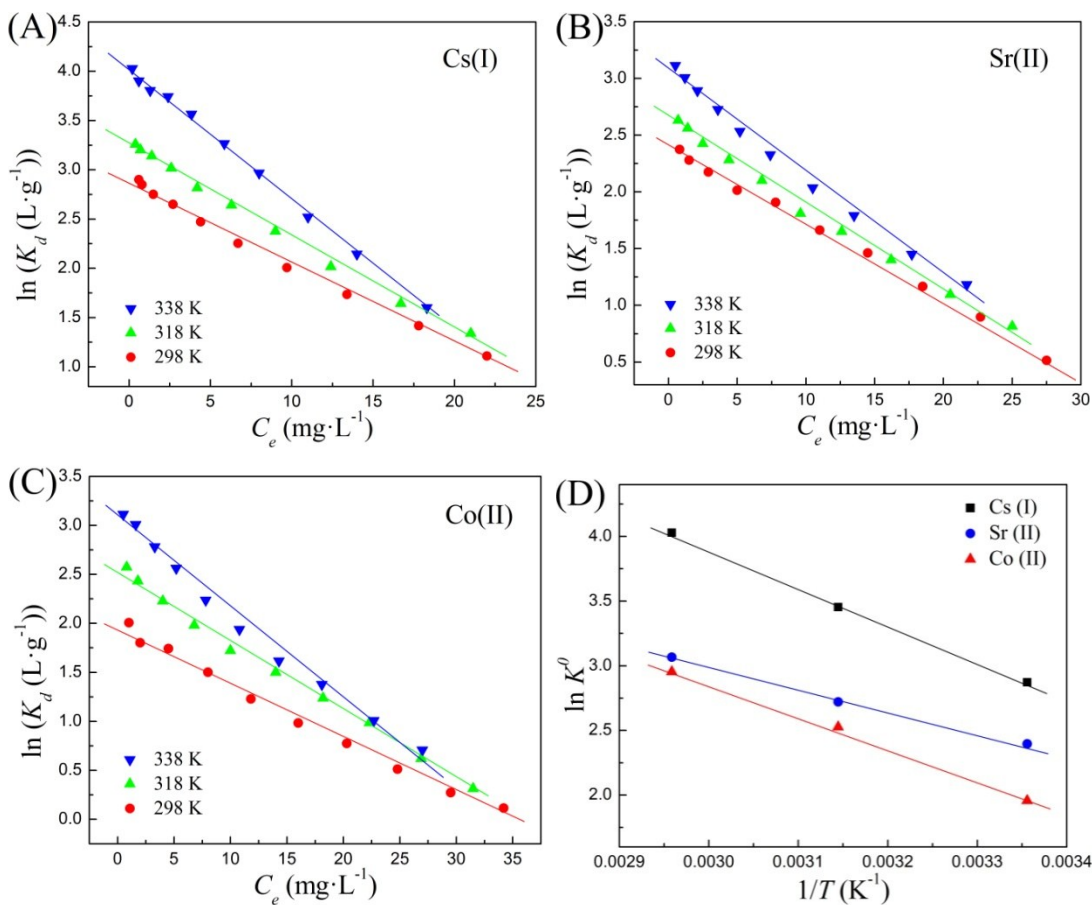
80



81

82 **Fig. S4.** Effect of pH on Cs(I), Sr(II) and Co(II) adsorption with different ionic strengths.
 83 $m/V = 0.5 \text{ g} \cdot \text{L}^{-1}$, $T = 298 \text{ K}$, $C_{initial} = 20 \text{ mg} \cdot \text{L}^{-1}$ for all cations.





89

90

91 **Fig. S6.** Linear plots of $\ln K_d$ versus C_e for the adsorption of Cs(I) (A), Sr(II) (B) and
 92 Co(II) (C). Linear plots of $\ln K^0$ versus $1/T$ for the radionuclide adsorption (D). $pH = 6.0 \pm$
 93 0.1 , $m/V = 0.5 \text{ g}\cdot\text{L}^{-1}$, $I = 0.01 \text{ M NaCl}$.

94 **References**

- 95 1. Y. S. Ho and G. McKay, *Process Biochem.*, 1999, **34**, 451–465.
- 96 2. C. H. Wu, *J. Hazard. Mater.*, 2007, **144**, 93–100.
- 97 3. F. A. Digiano, G. Baldauf, B. Frick and H. Sontheimer, *Chem. Eng. Sci.*, 1978, **33**,
- 98 1667–1673.